Less than 50% sublattice polarization

in an insulating $S =3/2$ kagomé antiferromagnet at T≈0

S.-H. Lee[1,3], C. Broholm[2,3], M. F. Collins[4], L. Heller[4], A. P. Ramirez[5], C. Kloc[5,6], E.

Bucher[5,6], R. W. Erwin[3], and N. Lacevic[2]

[1]*University of Maryland, College Park, MD 20742*

[2]*Department of Physics and Astronomy, The Johns Hopkins University, Baltimore, MD 21218*

[3]*National Institute of Standard and Technology, Gaithersburg, MD 20899*

[4]*Department of Physics and Astronomy, McMaster University, Hamilton, Ontario, L8S 4M1,*

Canada

[5]*Lucent Technologies, Bell Laboratories, Murray Hill, NJ 07974*

[6]*University of Konstanz, Konstanz 7750, Germany*

Abstract

We have found weak long range antiferromagnetic order in the quasi-two-dimensional insulating oxide $KCr_3(OD)_6(SO_4)_2$ which contains Cr^{3+} $S =3/2$ ions on a kagomé lattice. In a sample with ≈76% occupancy of the chromium sites the ordered moment is $1.1(3)\mu_B$ per chromium ion which is only one third of the Néel value $g\mu_B S = 3\mu_B$. The magnetic unit cell equals the chemical unit cell, a situation which is favored by inter-plane interactions. Gapless quantum spin-fluctuations ($\Delta/k_B < 0.25$K) with a bandwidth of 60K $>>$ T$_N$ = 1.6K are the dominant contribution to the spin correlation function, $\mathcal{S}(Q,\omega)$ in the ordered phase.

PACS numbers: 71.30.+h, 72.15.-v, 75.30.Kz

Typeset using REVTEX

I. INTRODUCTION

More often than not, local moments in insulating magnets acquire a finite expectation value, $< \vec{S} >$ at low temperatures. The only known exceptions are certain quasi-one-dimensional antiferromagnets (AFM) in which coupling between one dimensional units cannot overcome the tendency of each unit to form a cooperative quantum mechanical singlet. It is of great interest then to identify and study higher dimensional "moment free" insulating spin systems. We have made some progress towards this objective by identifying a quasi-two-dimensional magnet in which $| < \vec{S} > |$ is only $0.4(1) \times S$, where S is the spin quantum number of the magnetic ion.

The material in question is $KCr_3(OD)_6(SO_4)_2$, a quasi-two-dimensional AFM in which $S = 3/2$ Cr^{3+} ions occupy weakly interacting kagomé lattices. Quasi-two-dimensional AFM's containing spins on kagomé lattices are likely to have reduced values of $| < \vec{S} > |$ as a consequence of the weak connectivity and triangular motif of the lattice. For Heisenberg spins for example it is known that $| < \vec{S} > |/S \rightarrow 1$ for $S \rightarrow \infty$ and $T \rightarrow 0$ [1–8] whereas $| < \vec{S} > | = 0$ for $S = 1/2$ [9]. The critical value of S below which a moment free magnet exists at T=0 is however unknown [6].

Only a few AFM kagomé systems have been studied so far. $SrCr_{9p}Ga_{12-9p}O_{19}$ is a quasi-two-dimensional oxide containing antiferromagnetically interacting $S = 3/2$ Cr^{3+} ions in kagomé bilayers [10–14]. The material exhibits predominantly dynamic spin correlations although a spin-glass-like transition at $k_B T_g/J \approx 0.03$ causes condensation of weak two-dimensional static correlations with an ordered moment corresponding to $| < \vec{S} > | = 0.63(5)S$ and a correlation length of order twice the spin-spin separation [14–16]. There are also recent reports of short range magnetic order in $D_3OFe_3(OH)_6(SO_4)_2$ [17]. In contrast the Fe-jarosites $AFe_3(OH)_6(XO_4)_2$, with A=K, Na, Tl and X=S or Cr which realize a $S = 5/2$ kagomé AFM all have been found to develop long range order at low temperatures with ordered moments $| < \vec{S} > | \approx 0.7S$ [18,19].

In this paper we report experiments characterizing static and dynamic spin correlations

in the $S = 3/2$ jarosite kagomé lattice $KCr_3(OD)_6(SO_4)_2$. Our principal result is that long range order similar to that found in the $S = 5/2$ jarosite systems does develop but the spin polarization, $| < \vec{S} > |$, is only 0.4(1) times the Néel value, S. Quantum fluctuations account for the remaining spin of the Cr^{3+} ions. The bandwidth of the fluctuation spectrum is approximately 6 meV and we place an upper bound of 0.03 meV on any gap in the spectrum.

II. EXPERIMENTAL DETAILS

The neutron scattering measurements were carried out on thermal neutron triple axis spectrometers at the NIST reactor. Measurements were taken with fixed incident neutron energies of 13.7meV or 5meV using PG or Be as filters in the incident beam. Because important conclusions of this paper come from absolute measurements of the neutron scattering cross section, details of how we normalize scattering intensities from a powder sample are given in appendix A.

A 2.8g powder sample of $KCr_3(OH)_6(SO_4)_2$ and a 6g powder sample of $KCr_3(OD)_6(SO_4)_2$ were synthesized using previously published methods [20]. We denote these samples A and B respectively. Powder neutron scattering confirmed that the samples were single phase with the hexagonal alunite structure and low temperature lattice parameters a=7.2371 Å and c=16.9544 Å. Fig. 1 shows $T = 20$ K diffraction data from sample B with the Rietveld fit superimposed. In sample A the Cr^{3+} occupancy was 100% as determined from the slope of the inverse high temperature Curie-Weiss susceptibility versus T. In sample B prompt gamma activation analysis, refinement of powder neutron scattering (see Table 1 and Fig. 1) and chemical analysis indicated Cr^{3+} occupancy of 76(5)% whereas high temperature susceptibility measurement indicated 90% Cr occupancy. Unfortunately problems with stoichiometry are not uncommon in this complicated class of materials [21]. All neutron scattering experiments reported here were performed on the deuterated sample B.

The chromium lattice in $KCr_3(OD)_6(SO_4)_2$ is illustrated in Fig 2. A formula unit contains

three kagomé planes of chromium ions stacked along the c-axis. Neighboring kagomé planes (one shown with solid lines, another with dashed lines) are displaced by $(\frac{2}{3}, \frac{1}{3}, \frac{1}{3})$. A, B and C indicate three sublattices of the magnetic structure to be discussed later. Cr^{3+} ions are coordinated by six oxygen atoms located at the vertices of trigonally distorted octahedra [18,22]. Neighboring octahedra share one oxygen atom which is expected to mediate the strongest exchange interaction in the system between neighboring chromium ions separated by $d = 3.624$ Å in a kagomé plane. Susceptibility measurements on samples A and B showed Curie-Weiss temperatures, Θ_{CW}, of -70(5)K and -54(2)K respectively. If nearest neighbor exchange in the kagomé lattices indeed dominate, this corresponds to a bond strength $J = (3k_B|\Theta_{CW}|/\tilde{z}S(S+1)) = 1.2(1)meV$ where $\tilde{z} = 4n_{Cr}/9$ is the average nearest neighbor coordination (n_{Cr} is the number of chromium atoms per unit cell determined from Rietveld analysis and listed in Table 1). Other potentially significant exchange interactions in order of the strengths expected are the interplane coupling (Cr-K-Cr, d=6.025(1)Å) and the second nearest intraplane interaction (Cr-O-K-O-Cr, d=6.268(1)Å).

III. EXPERIMENTAL RESULTS

A. Antiferromagnetic long-range-order

Fig. 3 shows the temperature dependence of magnetic neutron diffraction at $Q = (012)$ and specific heat, C/T, which reveal a magnetic phase transition at $T_N = 1.8$ and 1.55K $\ll \Theta_{CW}$ for samples A and B respectively. The entropy change between 0.2K and 2.9K is only $0.15R\ln(2S+1)$ and $0.16R\ln(2S+1)$ respectively indicating that the ordered moment in these samples may be small and/or there may be substantial short range order above the Néel temperature. Note that in contrast to $D_3OFe_3(OH)_6(SO_4)_2$ [17] where impurities induce long range magnetic order, it is our cleanest sample, A, which has the most pronounced specific heat anomaly at T_N. This indicates that long range order is the clean limit low T state of $KCr_3(OD)_6(SO_4)_2$.

Fig. 4 shows low temperature magnetic diffraction data for sample B. The data was taken without final energy analysis and with an incident neutron energy, $E_i = 13.7$ meV, which far exceeds the energy range with appreciable inelastic magnetic scattering. The data therefore probes the equal time spin correlation function $\mathcal{S}(Q) = \int_{-\infty}^{\infty} \mathcal{S}(Q, \omega) \hbar d\omega$. The two frames show low temperature (T=0.4K) data with two different backgrounds subtracted. Using diffraction data from immediately above the Néel temperature (T=3.6K) as a background yields simply resolution limited magnetic Bragg diffraction indicating that the low temperature phase has AFM order. From comparing the line shapes of magnetic and nuclear Bragg peaks we conclude that the AFM correlation length exceeds 500 Å. Magnetic Bragg peaks occur at the same values of Q as nuclear Bragg peaks which implies that the chemical unit cell described above is also a unit cell for the magnetic structure. This implies that all triangles of spins which are connected by in-plane Bravais vectors of the crystal have equivalent spin orientations which we denote by A, B, and C. To determine the actual spin directions and the relative orientation of spins in neighboring kagomé planes we compared the measured Bragg intensities to those calculated for specific model structures. Table 2 makes the comparison to the spin configuration shown in Fig. 2 (a). In this structure, spins labeled by A, B, and C were taken to lie within the basal plane and to be rotated 120° with respect to one another. Subsequent kagomé layers are oriented so that each interplane triangle of chromium ions, such as those shaded in Fig. 2, contains all three spin orientations : A, B, and C. This structure provides the best account of the measured intensities out of 72 high symmetry spin configurations which were examined. The ordered moment determined from this analysis was $|M| = 1.1(3)\mu_B$ per occupied chromium site which if $g \approx 2$ and $S = 3/2$ implies that $| < \vec{S} > | = 0.4(1)S$. Note that the error bar quoted here includes the uncertainty associated with other choices of the interlayer registry which also provide a reasonable account of the diffraction data.

B. Equal-time short-range spin correlations

Since the long range ordered moment is small, sum-rules imply that we should find static or dynamic short range order which accounts for the remaining spin on Cr^{3+} ions. This aspect of the problem is examined in Fig. 4 (b) which shows diffraction data similar to those discussed above, though this time using T=50K$\approx \Theta_{CW}$ data for background subtraction. At T=50K we expect that magnetic scattering is almost Q-independent in the limited Q-range of the experiment. This is also the case for the thermally activated inelastic phonon scattering which is present in the high temperature data as well [23]. In Fig. 4 (b) these terms are over-subtracted but the Q–dependence of the difference data should follow that of the low temperature equal time correlation function $\mathcal{S}(Q)$. For the purpose of comparisons to theory we determined the base-line for $\mathcal{S}(Q)$ by requiring that the data (including magnetic Bragg peaks) satisfy the total moment sum rule $3 \times \int dQ Q^2 \mathcal{S}(Q)/\int dQ Q^2 = n_{Cr}(g/2)^2 S(S+1)$ using $n_{Cr} = 6.9$ as derived from powder diffraction. The most striking feature of the data is the unusually small fraction of the equal time correlation function which is associated with magnetic Bragg peaks. The result indicates that most of the chromium spin in this material remain spatially disordered down to T=0.4K.

C. Energy resolved magnetic neutron scattering

It is important to determine whether the short-range-order is static or dynamic. To settle this question we used the full triple axis configuration of the neutron spectrometer to measure the low temperature (T=70mK) spectrum of magnetic fluctuations at two values of Q. The result is shown in Fig. 5. Contributions to the detector count rate not associated with inelastic scattering from the sample were measured and subtracted as described in the figure caption. Integrating the data over $\hbar\omega$ we obtained the values for $\mathcal{S}(Q)$ shown with solid symbols in Fig. 4 (b). Inelastic scattering with 0.4meV$< \hbar\omega < 10$meV clearly accounts for most of the equal time correlation function and hence we may conclude that the short

range order in $KCr_3(OD)_6(SO_4)_2$ is mostly dynamic in origin. From the energy spectra shown in Fig. 5 we estimate a magnetic bandwidth of approximately 6meV. In addition we can place an upper limit of 0.4meV on any gap, Δ, in the magnetic excitation spectrum. A stricter constraint on Δ is derived from the specific heat data of Fig. 3 where the absence of activated behavior for $T > 0.25$ K indicates that $\Delta > 0.03$ meV.

Further information on magnetic fluctuations is provided by the constant-$\hbar\omega$ scans shown in Fig. 6. The data display an asymmetric peak centered close to the strongest AFM Bragg point, $\vec{\tau} = (101)$. The peak progressively broadens as energy transfer is increased. The sharp leading edge and gradual decrease in intensity with increasing Q is indicative of low dimensional magnetic correlations [24]. Based on *inelastic* constant-Q and constant-$\hbar\omega$ scans we can also evaluate the a *lower bound* on the total fluctuating moment $3 \times \int \mathcal{S}(Q, \hbar\omega)Q^2 dQ \hbar d\omega / \int Q^2 dQ = 15$ per unit cell. This number is an appreciable fraction of the total moment sum $n_{Cr}(g/2)^2 S(S+1) \approx 26$ per unit cell which indicates that the spin system remains predominantly dynamic at low temperatures in this material.

IV. DISCUSSION

A. Magnetic structure

Having presented the experimental results we now turn to comparison with relevant theory. The type of magnetic order in $KCr_3(OD)_6(SO_4)_2$ is surprising. Quantum as well as classical theories of the kagomé magnet predict that the so-called $\sqrt{3} \times \sqrt{3}$ in-plane structure [Fig. 2 (b)] is favored over the "q=0" structure which we observe. In addition another kagomé related material $SrCr_{9p}Ga_{12-9p}O_{19}$ shows short range $\sqrt{3} \times \sqrt{3}$ type order [15,16]. It is therefore surprising to find q=0 type AFM order in $KCr_3(OD)_6(SO_4)_2$. We believe that interplane coupling plays an important role in stabilizing this type of order in jarosite systems. As is apparent from Fig. 2 (a), q=0 kagomé AFM layers can be stacked to take advantage of ferro- as well as antiferromagnetic nearest neighbor interlayer

7

coupling, but $\sqrt{3} \times \sqrt{3}$ layers cannot. The reason is that the $(\frac{2}{3}, \frac{1}{3})$ in-plane translation between neighboring kagomé planes is incompatible with the periodicity of the $\sqrt{3} \times \sqrt{3}$ magnetic structure and it is therefore impossible to arrange for all interplane triangles of spins to contain all three spin orientations A, B, and C as required to satisfy interlayer coupling. Indeed, all jarosite kagomé systems studied so far have q=0 type in-plane AFM order. Interplane coupling also controls another aspect of the three dimensional magnetic structure : the length of the primitive magnetic unit cell in the c direction: Three identical but shifted q=0 layers can be stacked to satisfy AFM interplane coupling. For ferromagnetic interplane coupling, however, it is favorable to include time reversed copies of each of these three layers in the stack which leads to a six layer sequence and a doubling of the unit cell in the c-direction. Such unit cell doubling is actually observed for $KFe_3(OH)_6(SO_4)_2$ [18].

B. Comparison to spin wave theory

We have compared our inelastic data to specific models for dynamic correlations in the kagomé AFM. Several authors have considered spin waves in a long ranged ordered classical kagomé magnet and there are a few unusual features to note. As a consequence of a local continuous degree of freedom (the weather vane mode) spin wave theories to lowest order in $1/S$ yield a zero energy mode of excitations for all $\vec{Q}$. Furthermore it can be shown that all classical long range ordered ground states lead to the same dispersion relation for the finite energy modes. We used the results of Harris et al. [8] to calculate the inelastic neutron scattering cross section associated with the finite energy modes of the =0 structure [25]. The calculated cross section was convoluted with the experimental energy resolution function and is shown as dashed lines in Fig. 6. The comparison involves only a single adjustable parameter which is the overall scale factor. The exchange constant was fixed to 1meV, the value extracted from high temperature susceptibility measurements. Simple lowest order two dimensional spin wave theory clearly cannot account well for the data. Specifically the sharp features predicted by the theory are absent in the data. This is actually quite unusual

for two dimensional magnets. The qualitative features of spin dynamics in La_2CuO_4 are for example very well described by such theories [26].

C. Equal-time spin correlations

Theoretical predictions are also available for the equal time correlation function $\mathcal{S}(Q)$. We compare these to our data in Fig. 4. The dotted line is the result of a Monte Carlo study [27], and the dashed line resulted from a high-T expansion [8]. Given that the experimental data probe *low temperature* spin correlations it is surprising that apart from the magnetic Bragg peaks the high temperature expansion accounts quite well for the data. Evidently the frustration inherent to the kagomé AFM prevents much evolution of equal time correlations between high and low temperatures in $KCr_3(OD)_6(SO_4)_2$.

V. SUMMARY AND CONCLUSION

In summary, we have shown that long range AFM order exists below a second order transition at T_N=1.8K in the S =3/2 jarosite kagomé system $KCr_3(OD)_6(SO_4)_2$. The ordered structure preserves the chemical unit cell and we have argued that this type of structure is favored by interplane coupling. The ordered moment per Cr ion in a sample with 76% occupancy on the chromium sublattice is $1.1(3)\mu_B$ per occupied chromium site which is only one third of that corresponding to Néel order for S =3/2 spins. Concomitantly spin fluctuations are unusually strong in this system and cannot be accounted for by conventional spin wave theory. The inset to Fig. 5 summarizes $|<\vec{S}>|/S$ versus S for various kagomé systems studies so far. The data indicate that the weakly diluted S =3/2 kagomé AFM may be close to a T=0 quantum critical point separating a phase with $|<\vec{S}>| \neq 0$ from a phase with $|<\vec{S}>| = 0$ [6].

APPENDIX A: NORMALIZING POWDER NEUTRON SCATTERING DATA

1. Neutron Scattering Cross Sections

The magnetic neutron scattering cross section from a powder sample at wave vector transfer, Q, and energy transfer, $\hbar\omega$ can be written [28]

$$\frac{\mathrm{d}^2\sigma}{\mathrm{d}\Omega\mathrm{d}E'} = \frac{k'}{k}Nr_0^2 e^{-2W(Q)}\,2\mathcal{S}(Q,\omega) \tag{A1}$$

where $r_0 = 5.38$ fm, $e^{-2W(Q)}$ is the Debye Waller factor (which we generally take to be unity at low Q and low T), and $\mathcal{S}(Q,\omega)$ is the spherically averaged scattering function:

$$\mathcal{S}(Q,\omega) = \int \frac{d\Omega_{\hat{Q}}}{4\pi}\frac{1}{2}\sum_{\alpha\beta}(\delta_{\alpha\beta} - \hat{Q}_\alpha\hat{Q}_\beta)S^{\alpha\beta}(\vec{Q},\omega). \tag{A2}$$

The scattering function is given by

$$\mathcal{S}^{\alpha\beta}(\vec{Q},\omega) = |\frac{g}{2}f(\vec{Q})|^2\frac{1}{2\pi\hbar}\int dt e^{i\omega t}\frac{1}{N}\sum_{\vec{R}\vec{R}'} < S^\alpha_{\vec{R}}(t)S^\beta_{\vec{R}'}(0) > e^{-i\vec{Q}\cdot(\vec{R}-\vec{R}')} \tag{A3}$$

where $f(\vec{Q})$ is the magnetic form-factor of a single Cr ion [29].

The Bragg scattering cross section for a powder sample takes the form

$$\frac{\mathrm{d}\sigma}{\mathrm{d}\Omega} = N\sum_\tau \mathcal{I}(\tau)\delta(Q - \tau) \tag{A4}$$

where the summation is over reciprocal lattice vectors, τ, with different lengths. The Q–integrated nuclear scattering intensity is

$$\mathcal{I}_N(\tau) = \frac{v^*}{4\pi\tau^2}\sum_{|\vec{\tau}\,'|=\tau}|F_N(\vec{\tau}\,')|^2 \tag{A5}$$

where v^* is the volume of the reciprocal lattice unit cell and the structure factor is

$$F_N(\vec{Q}) = \sum_{\vec{d}} e^{-W_{\vec{d}}(\vec{Q})} b_{\vec{d}} \, e^{i\vec{Q}\cdot\vec{d}} \tag{A6}$$

For magnetic Bragg scattering the Q–integrated intensity is

$$\mathcal{I}_m(\tau) = r_0^2 \frac{v^*}{4\pi\tau^2} \sum_{|\vec{\tau}\,'|=\tau} |\frac{g}{2}f(\vec{\tau}\,')|^2 (|\vec{F}_M(\vec{\tau}\,')|^2 - |\hat{\tau}\cdot\vec{F}_M(\vec{\tau}\,')|^2), \tag{A7}$$

where the magnetic vector structure factor is given by

$$\vec{F}_M(\vec{Q}) = \sum_{\vec{d}} e^{-W_{\vec{d}}(\vec{Q})} < \vec{S}_{\vec{d}} > e^{i\vec{Q}\cdot\vec{d}} \tag{A8}$$

2. Normalizing the measured Intensities

The detector count rate is related to the scattering cross section through an expression of the form:

$$I(Q, \hbar\omega) = \mathcal{C}(\hbar\omega) \int dQ' \hbar d\omega' \mathcal{R}_{Q\omega}(Q - Q', \omega - \omega') \frac{d^2\sigma}{d\Omega dE'}(Q', \hbar\omega'), \tag{A9}$$

where the spectrometer resolution function is normalized to unity:

$$\int dQ' \hbar d\omega' \mathcal{R}_{Q\omega}(Q - Q', \omega - \omega') = 1 \tag{A10}$$

The resolution function and the energy dependence of $\mathcal{C}(\hbar\omega)/\mathcal{C}(0)$ can be calculated given the spectrometer set up [30]. For experiments with fixed incident energy it is a good approximation to use

$$\frac{\mathcal{C}(\hbar\omega)}{\mathcal{C}(0)} = (\frac{k'}{k})^2 \sqrt{\frac{(2k')^2 - \tau_A^2}{(2k)^2 - \tau_A^2}}, \tag{A11}$$

where k and k' are the incident and scattered neutron wave vectors, and $\vec{\tau}_A$ is the reciprocal lattice vector of the Bragg reflection being used as analyzer. The value $\mathcal{C}(0)$ depends on many factors such as the neutron flux, monochromator and analyzer reflectivities, collimator transmissions, and detector efficiencies. We determined $\mathcal{C}(0)$ by measuring the Q–integrated intensity of nuclear Bragg peaks with known values of $\mathcal{I}_N(\tau)$:

11

$$NC(0) = \frac{\int I_{\text{Bragg}}(Q - \tau, \hbar\omega)dQ\hbar d\omega}{\mathcal{I}_N(\tau)} \tag{A12}$$

With this number it is straight forward to derive absolute values of $\mathcal{I}_M(\tau)$ and $\mathcal{S}(Q, \hbar\omega)$ from the detector count rates associated with magnetic scattering:

$$\mathcal{I}_M(\tau) = \frac{1}{NC(0)}\int I_{\text{Bragg}}(Q, \hbar\omega)dQ\hbar d\omega \tag{A13}$$

$$\mathcal{S}(Q, \omega) \approx \frac{1}{NC(0)r_0^2}(\frac{k}{k'})^3\sqrt{\frac{(2k)^2 - \tau_A^2}{(2k')^2 - \tau_A^2}}\frac{1}{2}I(Q, \hbar\omega). \tag{A14}$$

Resolution smearing was neglected in the last expression.

TABLES

TABLE I. Positions within space group R$\bar{3}$m and occupancies per unit cell of atoms in KCr$_3$(OD)$_6$(SO$_4$)$_2$ at T=20K. The numbers were derived from the data shown in Fig. 1 by Rietveld analysis using GSAS [31]. Isotropic Debye-Waller factors, $\exp(- <u^2> Q^2)$, were used and the resulting overall reduced $\chi^2 = 3.8$.

	Site	x	y	z	n/f.u.	$\sqrt{<u^2>}/\text{Å}$
K	3b	0	0	0	3	0.090(5)
Cr	9d	0	0.5	0.5	6.9(2)	0.072(6)
O	18h	0.1282(2)	0.2564(3)	0.1341(1)	16.8(3)	0.072(2)
D	18h	0.1961(2)	0.3922(5)	0.1084(2)	13.8(3)	0.106(2)
H	18h	0.1961(2)	0.3922(5)	0.1084(2)	4.2(1)	0.106(2)
S	6c	0	0	0.3061(4)	5.73(9)	0.065(5)
O	6c	0	0	0.3903(2)	5.8(2)	0.075(3)
O	18h	0.2218(2)	0.4436(3)	−0.0573(1)	17.4(3)	0.077(2)

TABLE II. The measured and calculated Q–integrated intensities of Bragg peaks for $KCr_3(OD)_6(SO_4)_2$ powder sample B. Magnetic and nuclear peaks were measured with the same experimental configuration. Magnetic Bragg intensities were obtained from the difference between the scattering intensity at 0.4K and 3.6K shown in Fig. 4 (a). $\mathcal{I}_M^{cal}(\tau)$ was calculated using Eq. (A7) for the spin configuration shown in Fig. 2 with $(g/2) < \vec{S}_{\vec{d}} >= 0.55$. Comparing measurement to calculation we obtain a residual coefficient $R = \sum_\tau |\mathcal{I}^{obs}(\tau) - \mathcal{I}^{cal}(\tau)| / \sum_\tau \mathcal{I}^{obs}(\tau) = 0.17$. For nuclear Bragg peaks we got $R = 0.14$ when comparing $\mathcal{I}_N^{obs}(\tau)$ to $\mathcal{I}_N^{cal}(\tau)$. The latter values were calculated from Eq. (A5) and Table 1.

$\vec{\tau}$ (h,k,l)	Q^{obs} (Å^{-1})	$\mathcal{I}_M^{obs}(\tau)$ (10^{-18} m)	$\mathcal{I}_M^{cal}(\tau)$ (10^{-18} m)	$\mathcal{I}_N^{obs}(\tau)$ (10^{-18} m)	$\mathcal{I}_N^{cal}(\tau)$ (10^{-18} m)
1 0 1	1.070	0.061(6)	0.0581	0.32(3)	0.313
0 0 3	1.115	-	-	2.21(4)	1.029
0 1 2	1.240	0.038(6)	0.0419	0.03(3)	0.203
1 1 0	1.731	-	0.0065	0.06(1)	0.165
1 0 4	1.791	0.019(6)	0.0184	0.32(3)	0.261
2 0 $\bar{1}$, 1 1 3	2.063	0.01(1)	0.0119	4.8(1)	4.683
1 0 $\bar{5}$, 2 0 2	2.139	-		4.2(1)	3.632
0 0 6	2.222	-	-	0.17(5)	0.158
2 0 $\bar{4}$	2.498	-	-	0.42(1)	0.194
2 0 5, 2 1 $\bar{2}$,1 0 7	2.753	-	-	14.45(6)	14.057
3 0 0, 2 1 4	3.018	-	-	1.16(3)	0.977
3 0 $\bar{3}$, 2 1 $\bar{5}$	3.216	-	-	2.58(6)	3.667
2 0 $\bar{7}$	3.285	-	-	1.45(6)	1.710
2 2 0	3.476	-	-	2.9(1)	3.290

REFERENCES

[1] D.A. Huse et al., Phys. Rev. **B 45**, 7536 (1992).

[2] D. L. Huber et al., Phys. Rev. **B 47**, 3220 (1993).

[3] I. Ritchey et al., Phys. Rev. B**47**, 15342 (1993).

[4] E. F. Shender et al., Phys. Rev. Lett. **70**, 3812 (1993).

[5] P. Chandra et al., J. de Phys. I France **3** 591 (1993).

[6] S. Sachdev, Phys. Rev. B**45**, 12377 (1992).

[7] A. Chubukov, Phys. Rev. Lett. **69**, 832 (1992).

[8] A.B.Harris et al., Phys. Rev. B **45**, 2899 (1992)

[9] R.R.P Singh et al., Phys. Rev. Lett. **68**, 1766 (1992).

[10] X. Obradors et al., Solid State Commun. **65**, 189 (1988).

[11] A.P.Ramirez et al., Phys. Rev. Lett **64**, 2070 (1990).

[12] B.Martínez et al., Phys. Rev. B **46**, 10786 (1992).

[13] Y. J. Uemura et al., Phys. Rev. Lett. **73**, 3306 (1994).

[14] S.-H. Lee, et al., Phys. Rev. Lett. **76** 4424 (1996).

[15] S.-H. Lee et al. Europhys. Lett. **35** 127 (1996).

[16] C. Broholm et al., Phys. Rev. Lett **65**, 3173 (1990).

[17] A. S. Wills, A. Harrison, S. A. M. Mentink, T. E. Mason, an Z. Tun, preprint (1997).

[18] M. G. Townsend et al., Phys. Rev. **B33**, 4919 (1986).

[19] M. F. Collins, unpublished.

[20] J. E. Dutrizac et al., Can. Mineral. **14**, 151 (1976).

[21] J. A. Ripmeester, C.I.Ratcliffe, J.E.Dutrizac and J.L.Jambor, Can. Mineral. **24**, 435 (1986).

[22] R. Wang et al., Acta Crystallogr. **18**, 249 (1965); M. Takano et al., J. Phys. Soc. Japan **30**, 1049 (1971).

[23] The one phonon scattering cross section rises as Q^2. However, for a powder sample in the small Q limit inelastic phonon scattering mainly occurs in combination with an incoherent elastic scattering event resulting in an almost Q-independent double scattering process.

[24] B.E. Warren, Phys. Rev, **59** 693 (1941).

[25] S.-H. Lee, "Frustration, Order or not Order ? – a Neutron Scattering Study of Geometrically Frustrated Antiferromagnets", Ph. D. Thesis, Johns Hopkins University, unpublished (1996).

[26] S. M. Hayden, G. Aeppli, R. Osborn, A. D. Taylor, T. G. Perring, S.-W. Cheong, Z. Fisk, Phys. Rev. Lett. **67**, 3622 (1992).

[27] J.N. Reimers et al., Phys. Rev. **B 48**, 9539 (1993).

[28] We use the notation of S.W. Lovesey, *Theory of Neutron Scattering from Condensed Matter*, Clarendon Press., Oxford (1984).

[29] A. J. Freeman and R. E. Watson, Acta. Cryst. **14**, 231 (1961).

[30] N. D. Chesser and J. D. Axe, Acta Cryst. A **29**, 160 (1973).

[31] A.C. Larson and R.B. Von Dreele, Los Alamos National Laboratory Report No. LAUR 86-748.

FIGURES

FIG. 1. Powder diffraction data from sample B at $T = 20$ K taken on the 32 detector powder diffractometer BT 1 at NIST. We used the Cu (311) monochromator with $\lambda = 1.540$ Å and collimations $15' - 20' - 7'$. The line through the data shows the Rietveld fit which led to the structural parameters shown in Table 1. The bottom panel shows the difference between model and data.
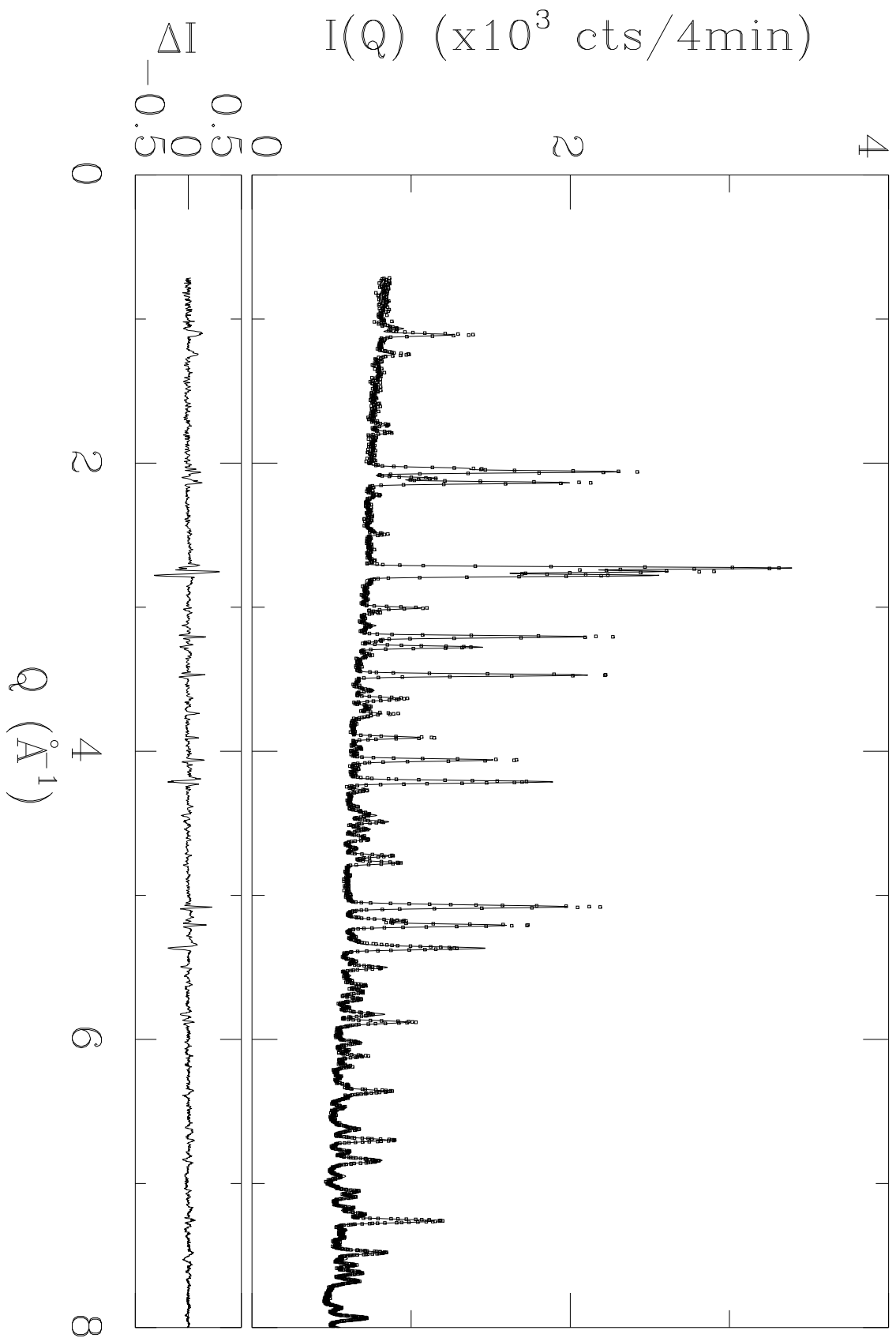
FIG. 2. Stacked kagomé lattices as they occur in jarosites. A, B, and C denote three magnetic sublattices. (a) is the spin configuration we propose for $KCr_3(OD)_6(SO_4)_2$ which satisfies inter-plane exchange interactions (shaded triangle). (b) Shows that a stacking of kagomé layers with the $\sqrt{3} \times \sqrt{3}$ AFM structure cannot satisfy inter-plane coupling.
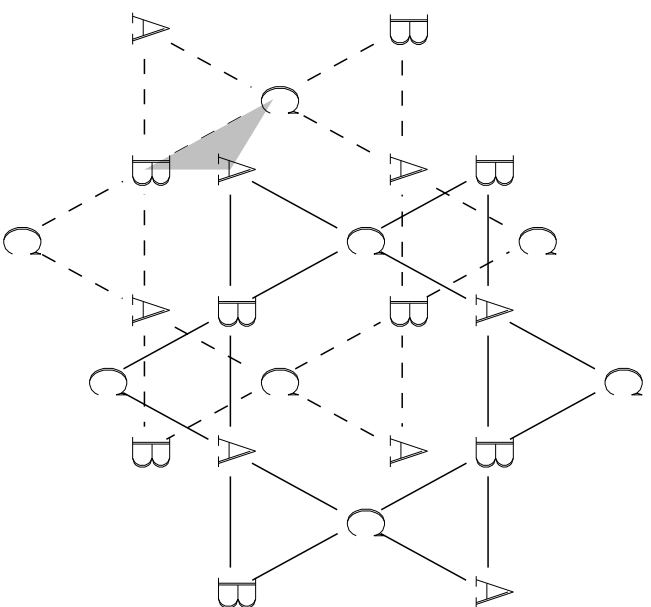
FIG. 3. (a) Temperature dependence of the magnetic Bragg intensity at $Q = (012)$ which is proportional to the squared staggered magnetization. (b) Temperature dependence of the specific heat divided by temperature for two samples with different Cr concentration in the kagomé layers. A 100% Cr^{3+} and B: 75-90% Cr^{3+}.

FIG. 4. Difference between low and high temperature neutron diffraction data. The data were obtained with $E_i = 13.7$meV, collimations $40' - 36' - 36'$ and no analyzer. (a) Shows I(0.4K)-I(3.6K) probing spin correlations which develop between T=3.6K and T=0.4K. (b) Shows I(0.4K)-I(50K) which is a measure of the entire low temperature equal time spin correlation function. The solid symbols were obtained by integrating the constant-Q scans shown in Fig. 5. Dotted and dashed lines are described in the text.
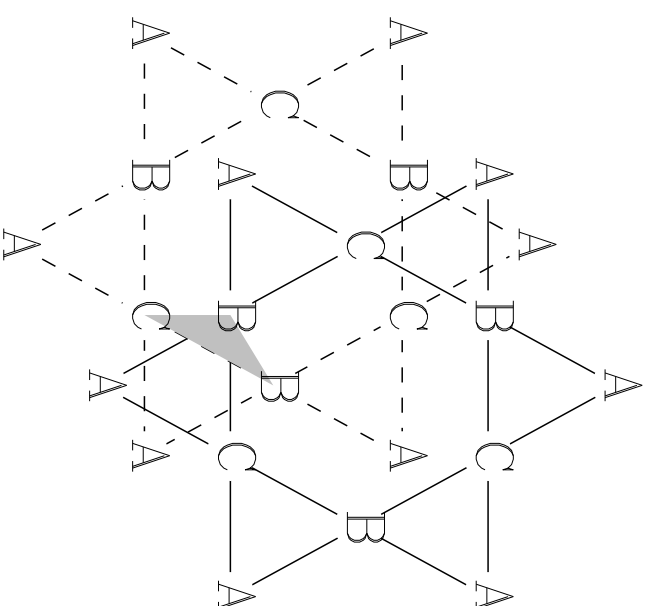
FIG. 5. Constant-Q scans at $Q = 1.1\text{Å}^{-1}$ (filled symbols) and $Q = 0.55\text{Å}^{-1}$ (open symbols). Triangles were obtained with E_i=5meV and collimations $60' - 40' - 80' - 80'$, circles with E_i=13.7meV and $60' - 20' - 40' - 40'$ and rectangles with E_i=14.7meV and collimations $60' - 20' - 40' - 40'$. Backgrounds were subtracted as follows : For $\hbar\omega \leq 0.7$meV we subtracted neutron energy gain data. For $\hbar\omega > 0.7$meV we subtracted data obtained with the analyzer rotated 10° from its reflection condition. The inset shows $| < \vec{S} > |/S$ versus S for various kagomé systems. Squares: $S = 5/2$ Fe-jarosite systems with long range order [18]; Open circles: frozen moment in the spin glass phase of $SrCr_{9p}Ga_{12-9p}O_{19}$ with p=0.92 and $S = 3/2$ [15]; Filled circle: long range ordered moment in the $S = 3/2$ Cr-jarosite $KCr_3(OD)_6(SO_4)_2$ with 76% occupancy of the kagomé lattice.

FIG. 6. Constant-$\hbar\omega$ scans at 0.5, 1.1, and 2 meV. The $\hbar\omega$=0.5meV scan was obtained with E_i=5meV and collimations $60' - 40' - 80' - 80'$. The $\hbar\omega$=1.1meV and $\hbar\omega$=2.0meV scans were obtained with E_i=13.7meV and collimations $60' - 20' - 40' - 40'$. The background subtraction scheme is described in the caption to Fig. 5. Solid lines are a single parameter fit to a spin wave theory described as in the text.

(a) AFM J' q=0

(b) $\sqrt{3} \times \sqrt{3}$